Title

Multiple Glass Transitions and Freezing Events of Aqueous Citric Acid

Journal

The Journal of Physical Chemistry A, 119(19)

ISSN

1089-5639

Authors

Bogdan, Anatoli
Molina, Mario J
Tenhu, Heikki
et al.

Publication Date

2015-05-14

DOI

10.1021/jp510331h

Peer reviewed

THE JOURNAL OF PHYSICAL CHEMISTRY A

Article

pubs.acs.org/JPCA

Multiple Glass Transitions and Freezing Events of Aqueous Citric Acid

Anatoli Bogdan,*[,†,‡,§] Mario J. Molina,[∥] Heikki Tenhu,[‡] and Thomas Loerting[†]

[†]Institute of Physical Chemistry, University of Innsbruck, Innrain 80-82, A-6020 Innsbruck, Austria

[‡]Laboratory of Polymer Chemistry, Department of Chemistry, University of Helsinki, Helsinki FI-00014, Finland

[§]Department of Physics, University of Helsinki, Helsinki FI-00014, Finland

[∥]Department of Chemistry and Biochemistry, University of California, San Diego, La Jolla, California 92093-0356, United States

ABSTRACT: Calorimetric and optical cryo-microscope measurements of 10−64 wt % citric acid (CA) solutions subjected to moderate (3 K/min) and slow (0.5 and 0.1 K/min) cooling/warming rates and also to quenching/moderate warming between 320 and 133 K are presented. Depending on solution concentration and cooling rate, the obtained thermograms show one freezing event and from one to three liquid−glass transitions upon cooling and from one to six liquid−glass and reverse glass−liquid transitions, one or two freezing events, and one melting event upon warming of frozen/glassy CA/H_2O. The multiple freezing events and glass transitions pertain to the mother CA/H_2O solution itself and two freeze-concentrated solution regions, FCS_1 and FCS_2, of different concentrations. The FCS_1 and FCS_2 (or FCS_{22}) are formed during the freezing of CA/H_2O upon cooling and/or during the freezing upon warming of partly glassy or entirely glassy mother CA/H_2O. The formation of two FCS_1 and FCS_{22} regions during the freezing upon warming to our best knowledge has never been reported before. Using an optical cryo-microscope, we are able to observe the formation of a continuous ice framework (IF) and its morphology and reciprocal distribution of IF/(FCS_1 + FCS_2). Our results provide a new look at the freezing and glass transition behavior of aqueous solutions and can be used for the optimization of lyophilization and freezing of foods and biopharmaceutical formulations, among many other applications where freezing plays a crucial role.

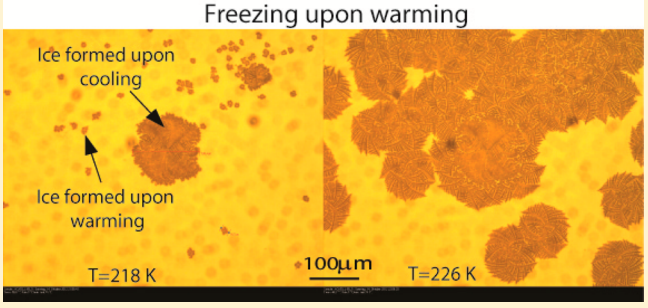

1. INTRODUCTION

Citric acid (CA), $C_6H_8O_7$, is a weak organic acid that is naturally encountered in a variety of fruits and vegetables, especially lemons and limes, and is commercially produced in very large amount by microbial fermentation of carbohydrates. The usual form of CA is CA-monohydrate, $C_6H_8O_7{\cdot}H_2O$, which is crystallized by the slow evaporation of water from cold saturated solutions, whereas anhydrous CA is crystallized from hot saturated solution.[1] CA by virtue of its hydroxyl −OH and carboxyl −COOH groups is capable to form hydrogen bonding between CA molecules themselves and with solvent H_2O molecules,[2,3] which results in a variety of unique properties of CA/H_2O solutions. Strong hydrogen bonding is believed to be a property that may prevent the crystallization of CA from cooled melt/solutions and be responsible for a liquid−glass transition[4,5] that is important for freeze-drying (lyophilization) and freezing of pharmaceutical formulations. CA is widely used in foods and beverages as a flavoring and preservative additive,[5,6] industry,[6−8] pharmaceutics as excipient[9] for freeze-dried formulations,[10] and in order to produce amorphous multicomponent excipients having high glass transition temperature, T_g, which could reduce or prevent protein denaturation in lyophilized formulations.[11,12] CA increases solubility of poorly water-soluble drugs[13,14] and efficiently maintains pH in the range from 3 to 6.2 that increases the stability of therapeutic proteins in frozen large scale formulations during storage.[15,16] CA is also used for the solubilization and sustained delivery of anti-HIV (human immunodeficiency virus) drug[17] and in tissue engineering (synthesis of biodegradable scaffold),[18−22] biochemistry, etc.

Although CA is widely used in the different fields of science, industry, and low temperature processing, there are still gaps in understanding of freeze-induced phase separation into pure ice and freeze-concentrated solution (FCS), glass transition behavior of formed FCS, and the morphology and reciprocal distribution of ice and glassy FCS in frozen solutions. In this article, we present the differential scanning calorimetry (DSC) and optical cryo-microscope (OC-M) results of the study of 10−64 wt % CA solutions subjected to different cooling and warming rates. Our results obtained from the combined DSC and OC-M measurements give a clear picture of how ice and FCSs of different concentrations are formed during the freezing

Special Issue: Mario Molina Festschrift

Received: October 13, 2014
Revised: December 1, 2014
Published: December 7, 2014

   dx.doi.org/10.1021/jp510331h | J. Phys. Chem. A 2015, 119, 4515−4523

upon cooling and subsequent warming and reveal a variety of liquid−glass and reverse glass−liquid transitions, which have not been observed before.

2. EXPERIMENTAL SECTION

We prepared 10−64 wt % CA solutions by mixing >99% anhydrous citric acid (Merck) with the corresponding amount of ultrapure water. The solutions of concentration larger than the solubility limit of ∼62 wt % CA at 295 K[23,24] were prepared by slow heating. We studied the phase transformations and glass transitions of CA/H_2O using a Mettler Toledo DSC 822 calorimeter at the scanning cooling/warming rate of 3, 0.5, and 0.1 K/min in the temperature region between 320 and 133 K. Such cooling rates are usually applied during the lyophilization of large scale food and biopharmaceutical formulations. For the DSC measurements, we loaded and then cold sealed a half-sphere solution drop in an aluminum (Al) crucible of 40 μL by volume. The mass and diameter of drops were ∼5−6 mg and ∼1.5 mm, respectively. We also performed measurements at 3 K/min upon warming of quenched CA/H_2O drops. To this end we placed an Al crucible with CA/H_2O drop into liquid N_2 and then immediately inserted the crucible into the precooled calorimeter. In this procedure, the cooling rate is estimated to be 100−1000 K/s. DSC calibration and details about measurements are described elsewhere.[25,26] To verify the reproducibility of results, we performed a number of repeated DSC measurements, which were of two types: (i) we sometimes measured the same drops 2−3 times, and (ii) we always performed measurements of 3−4 different drops of the same concentration.

To observe the freezing process in situ and the morphology of ice/FCS(s), we prepared ∼5−10 μm thick solution films ("2-dimensional" solutions)[27] and studied them with an optical cryo-microscope Olympus BX51 equipped with a Linkam cold stage and Linksys32 temperature control and video capture software. We performed optical cryo-microscope measurements at 3 and 5 K/min in the temperature region between 320 and 163 K.

3. RESULTS AND DISCUSSION

3.1. Cooling and Warming of CA/H_2O at 3 K/min. In Figure 1, we present cooling and warming thermograms obtained from 10−64 wt % CA solutions. In the cooling thermograms, an exothermic T_f peak indicates the latent heat of fusion emitted during freezing.[25,26] In the warming thermograms, an endothermic T_m peak is due to the absorption of latent heat during ice melting. The sharpness of the ice freezing T_f peak in the thermograms for 10−50 wt % CA indicates that the freezing process proceeds rapidly. Our numerous OC-M observations of frozen CA/H_2O solutions[27] show that such fast freezing process is always initiated from *one* ice nucleating event, as is demonstrated in Figure 2a,d. In supercooled solutions of this concentration range, the first nucleated critical ice embryo grows very rapidly and emits a large amount of latent heat of fusion. We surmise that the emitted heat raises the temperature of the surrounding liquid and prevents the nucleation of other critical ice embryos. In contrast, more concentrated solutions, namely, 55, 56, and 60 wt % CA, freeze from multiple ice nucleating events,[27] as is also demonstrated in Figure 2b. The 55, 56, and 60 wt % CA cooling thermograms contain a prolonged, broad freezing T_f peak (cf. Figure 1). Such prolonged freezing is caused by the steep increase of viscosity,

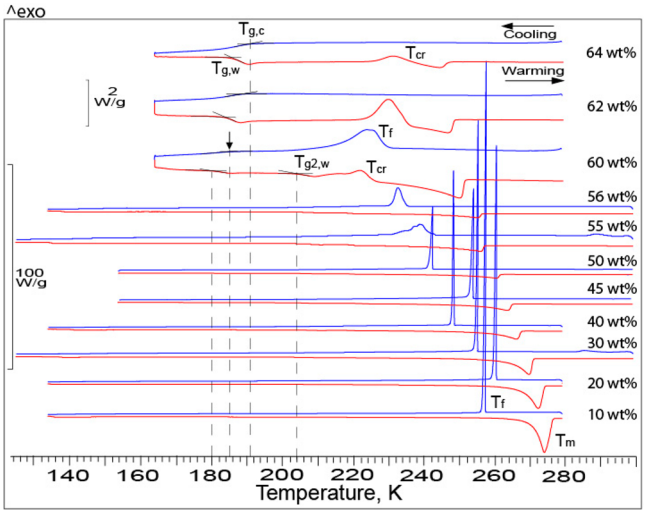

Figure 1. DSC cooling (upper blue lines) and warming thermograms (lower red lines) obtained from 10−64 wt % CA drops at the scanning rate of 3 K/min. Horizontal arrows mark the direction of programmed temperature change. T_f and T_m mark exothermic ice freezing and endothermic ice melting peaks, respectively. $T_{g,c}$ marks a liquid−glass transition upon cooling and $T_{g,w}$ and $T_{g2,w}$ reverse glass−liquid transitions upon warming (see text for details). T_{cr} marks freezing (ice crystallization) upon warming. Solution concentration is indicated. Scale-bars indicate heat flow through samples.

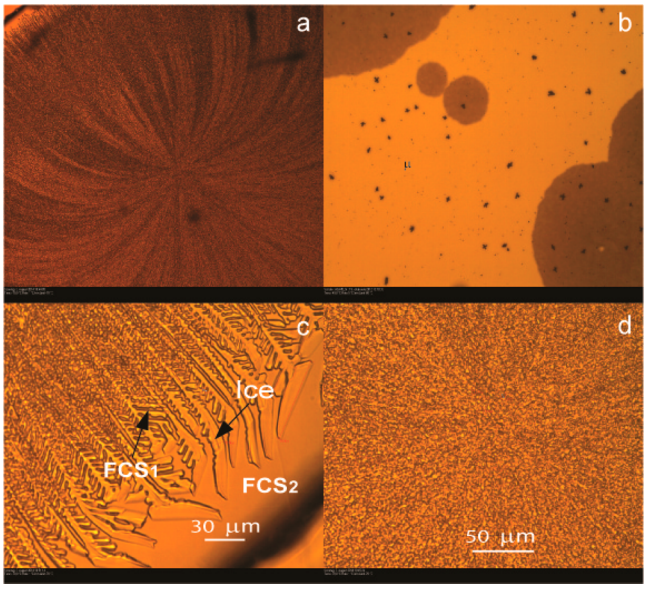

Figure 2. Optical cryo-microscope pictures of frozen CA/H_2O solution. (a) A picture demonstrates that freezing is initiated from a single ice nucleating event. Radial protuberances of different brightness are due to the different density of ice branches and channels of freeze-concentrated solution, FCS_1 (see also panel c). (b) Freezing of concentrated solution is initiated from multiple ice nucleating events. Dark spots are ice crystals formed by vapor deposition on an upper side of a cover glass. (c) Branches of a continuous ice framework (IF) formed from a single ice nucleating event shown in panel a. Arrows show ice in contact with a cover glass and channels of FCS_1 in between ice branches. A less concentrated freeze-concentrated solution, FCS_2, envelops the entire IF/FCS_1. (d) Magnification of the ice nucleation region from Panel a. Interweaved ice branches and FCS_1 channels are seen as bright and dark spots, respectively.

dx.doi.org/10.1021/jp510331h | J. Phys. Chem. A 2015, 119, 4515−4523

which progressively slows down ice growth and, consequently, reduces the emitting of the latent heat of fusion as temperature decreases. In this case the amount of the emitted heat per unit time is less than that withdrawn by the applied cooling rate of 3 K/min. As a result, the supercooling of surrounding liquid increases with decreasing temperature, and this results in the appearance of new ice nucleating events.

In our DSC measurements, CA/H_2O drops/solutions are placed on Al crucibles and, consequently, freeze heterogeneously. Figure 1 shows that the heterogeneous freezing temperature (T_f peaks) of 10−45 wt % CA is not a monotonic function of concentration. This freezing behavior differs from that of inorganic solutions, for example, $(NH_4)_2SO_4/H_2O$, in which a monotonous decrease of T_f is observed upon increasing solution concentration.[25] We suggest that the difference can be accounted for by concentration inhomogeneities in CA/H_2O, which result from the enhanced tendency of CA/H_2O to form molecular CA clusters at low temperature.[8,28−32] Supercooled CA/H_2O solutions can be viewed as arbitrarily distributed concentrated regions containing a large number of CA clusters and less concentrated regions with fewer CA clusters. Heterogeneous freezing is initiated at a point where the configuration of local electrical fields of the Al substrate and H_2O molecules favors the nucleation of critical ice embryo. Naturally, the onset of freezing will be governed by the warmest ice nucleating site on the Al substrate, which is in contact with a less concentrated patch within the solution. In contrast to freezing, the melting of ice is an equilibrium process, and therefore, the peak melting temperature, T_m, is a monotonic function of concentration, as is seen in Figure 1. Figure 1 also shows that in contrast to the sharp ice freezing T_f peaks, the ice melting T_m peaks are not sharp but occupy a large temperature region, which is warmer than that of T_f peaks, i.e., melting always occurs at temperature warmer than that of freezing. The melting of ice starts at the ice/FCS interface at very low temperature and gradually propagates to warmer temperatures as concentration decreases due to ice melting.

In the DSC method, a hallmark of glass transitions is a baseline step indicating a heat capacity change, ΔC_p.[33] An increase in heat capacity (upon heating) indicates a glass−liquid transition, whereas a decrease in heat capacity (upon cooling) indicates the reverse process, a liquid−glass transition. Figure 1 shows that the cooling thermogram of 60 wt % CA contains a prolonged ice freezing T_f peak and a liquid−glass transition with the onset at $T_{g,c} \approx 185$ K. Unexpectedly, in the warming scan for 60 wt % CA we find *two* glass−liquid transitions, $T_{g,w}$ and $T_{g2,w}$. Instead, we would expect that for each liquid−glass transition observed calorimetrically upon cooling there should be exactly one reverse glass−liquid transition upon warming at about the same temperature. In addition to the unexpected second glass−liquid transition we also observe a prolonged exothermic ice crystallization peak, T_{cr}, upon warming. To explain the T_{cr} transition we resort to simpler thermograms: In the cooling thermogram of 62 and 64 wt % CA, there is no freezing event but only a liquid−glass transition with the onset at $T_{g,c} \approx 189$ and 191 K, respectively. During the cooling of these solutions, their viscosity increases so steeply that it completely suppresses the freezing process. Upon subsequent warming above the reverse glass−liquid transition, $T_{g,w}$, the glass "melts" to a highly viscous liquid (HVL).[34] Upon further warming the viscosity of HVL decreases and ice starts crystallizing to produce an exothermic peak T_{cr}. The onset of ice crystallization is more than 40 K warmer than $T_{g,w}$, i.e., the HVL of CA/H_2O persists in a surprisingly large temperature window.

The thermograms of 10−60 wt % CA as displayed in Figure 1 do not give sufficient information for the comprehensive understanding of the freezing and thawing phenomena. In Figures 3 and 4, we present magnified cooling and warming

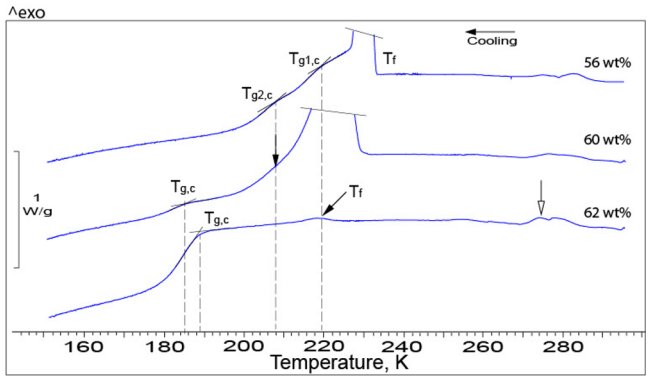

Figure 3. Magnified cooling thermograms of 56, 60, and 62 wt % CA obtained at 3 K/min. The cooling thermogram of 56 wt % CA is from Figure 1. $T_{g1,c}$, $T_{g2,c}$ and $T_{g,c}$ mark the onset of liquid−glass transitions. A vertical filled arrow marks $T_{g2,c}$ transition in 60 wt % CA thermogram. An open arrow marks a transition from anhydrous CA to CA-monohydrate.[35,36] In the 56 and 60 wt % CA thermograms, the ice freezing peak T_f is truncated to fit the figure.

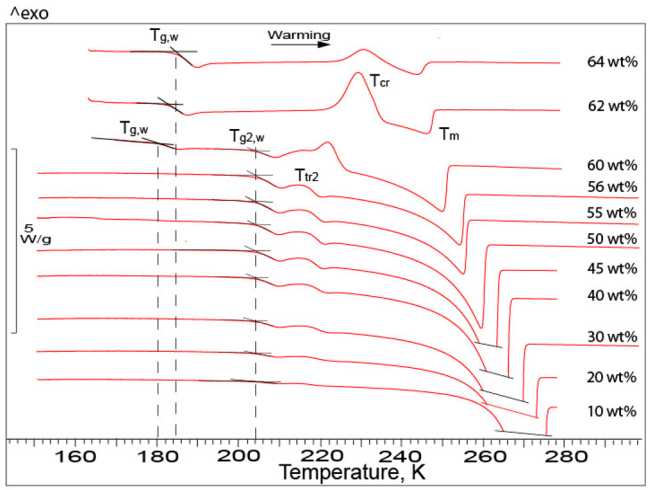

Figure 4. Magnified warming thermograms from Figure 1. $T_{g,w}$ and $T_{g,2w}$ mark the onset of glass−liquid transitions (see also Figures 1 and 3). T_{tr2} is a historical name of the second transition observed in the past during the warming of frozen hydrocarbon solutions (see text for details). Skewed lines truncate ice melting peaks, T_m, to fit the figure. The remaining symbols have the same meaning as in Figure 1.

thermograms, which reveal transitions not visible in Figure 1. In Figure 3, a subtle exothermic event around 280 K marked by an open arrow is most likely due to the transformation of anhydrous CA to CA-monohydrate upon cooling. It was reported that this transition occurs below 307 K, where CA monohydrate becomes more stable than anhydrous CA.[35,36] An alternative explanation of the exothermic peak around 280 K could have been the condensation of water vapor on the DSC lid during cooling.[37] The freezing of this condensed water would produce pure ice, which upon warming would start to melt at ~273 K producing a second ice melting peak. The twin

dx.doi.org/10.1021/jp510331h | J. Phys. Chem. A 2015, 119, 4515−4523

ice-melting peaks were indeed observed in the thermograms obtained upon warming of frozen gelatinized-starch.[37] However, in our case the warming thermograms reveal only one ice melting peak, T_m, which is due to the melting of ice surrounded by FCS (Figures 2 and 4). Further, we did not observe the exothermic event around 280 K in the cooling thermograms of pure water and other aqueous solutions, for example, $(NH_4)_2SO_4/H_2O$.[25] Thus, in Figure 3, the prolonged exothermic event around 280 K cannot be due to the condensation of water vapor on the DSC lid.

Figure 3 reveals an interesting shape of the T_f peak: while it is sharp at the onset of freezing it becomes broader at the low-temperature, indicating sluggish freezing.[27] In addition, the broad, inclined tail is carrying signatures for two liquid–glass transitions with the onset at $T_{g1,c} \approx 220$ and $T_{g2,c} \approx 208$ K, respectively. We observe the sluggish freezing process and the $T_{g1,c}$ and $T_{g2,c}$ transitions at the *same* onset temperatures in the cooling thermograms of *all* solutions of ≤56 wt % CA. Recently we reported that the $T_{g1,c}$ and $T_{g2,c}$ transitions are indicative of two freeze-concentrated solutions of different concentrations, FCS_1 and FCS_2, which are formed during freezing.[27] The FCS_1 is *maximally* freeze-concentrated and entangled with the twisted ice branches of a continuous ice framework, IF, whereas FCS_2 envelops the entire IF/FCS_1.[27] The mutual distribution of IF and (FCS_1 + FCS_2) is demonstrated in the pictures of frozen CA/H_2O in Figure 2. On the basis of our numerous in situ OC-M observations of freezing in supercooled CA/H_2O and sucrose/H_2O solutions, we reported that the sluggish freezing process proceeds in FCS_2 and it is terminated by a FCS_2–glass transition, $T_{g2,c}$, at low temperature.[27] Correspondingly, the FCS_1–glass transition at higher temperature is related to $T_{g1,c}$. Thus, upon cooling of 10–56 wt % CA solutions, one freezing event, T_f, and two liquid–glass transitions with the onset temperatures of $T_{g1,c} \approx 220$ and $T_{g2,c} \approx 208$ K are observed.

In Figure 4, we present magnified warming thermograms from Figure 1. It is seen that in 10–56 wt % CA thermograms, a reverse glass–liquid transitions, $T_{g2,w}$, and a second transition T_{tr2} are clearly visible. In the past, these transitions have been only observed upon warming of frozen hydrocarbon solutions.[38−51] Historically, they were called T_{tr1} and T_{tr2} transitions, where the former has been related to a glass–liquid transition. Recently, we reported that the T_{tr1} transition corresponds to the glass–liquid transition in the FCS_2 part of the sample. That is, it represents the $T_{g2,w}$ glass–liquid transition, which is the reversion of the liquid–glass transition, $T_{g2,c}$, observed upon cooling.[27] However, the T_{tr2} transition does not look like a genuine glass–liquid transition because of a clearly pronounced exothermic feature. The nature of the T_{tr2} transition has remained misunderstood for decades.[38−51] We demonstrated in videos, in which the freezing process was visualized in situ, that upon warming above $T_{g2,w}$ the terminated sluggish freezing of FCS_2 recommences and continues also in the temperature region of the T_{tr2} transition.[27] We concluded that the T_{tr2} transition is a net thermal effect produced by the heat capacity change ΔC_p of a reverse glass–FCS_1 transition, $T_{g1,w}$ and the latent heat of fusion emitted during the recommenced sluggish freezing of FCS_2.[27] One can see in Figure 4 that the onset temperatures of $T_{g2,w}$ and the temperature region of the T_{tr2} transition are well reproducible and independent of the initial solution concentration. We estimated the onset temperatures to be $T_{g2,w} \approx 204$ K and $T_{g1,w} \approx 217$ K.[27] Thus, upon warming of frozen 10–56 wt % CA solutions, two glass–liquid transitions, $T_{g2,w}$ and $T_{g1,w}$, one freezing, namely, the resumed freezing of FCS_2, and ice melting at T_m are observed.

In Figure 4, the thermograms of 62 and 64 wt % CA do not show the $T_{g2,w}$ and T_{tr2} (or $T_{g1,w}$) transitions because they do not freeze upon cooling (Figure 1), and consequently, no FCS_1 and FCS_2 are formed. Therefore, only a reverse glass–liquid transition of $T_{g,w}$ is observed upon warming. Further, Figure 3 shows that 62 wt % CA solution freezes only to a minor extent. The small amount of ice formed during freezing results in the formation of only a trace amount of FCS_1 and FCS_2, and so the $T_{g2,w}$ and $T_{g1,w}$ transitions are too subtle to be detectable with our DSC device. In Figure 5, we present OC-M pictures, which

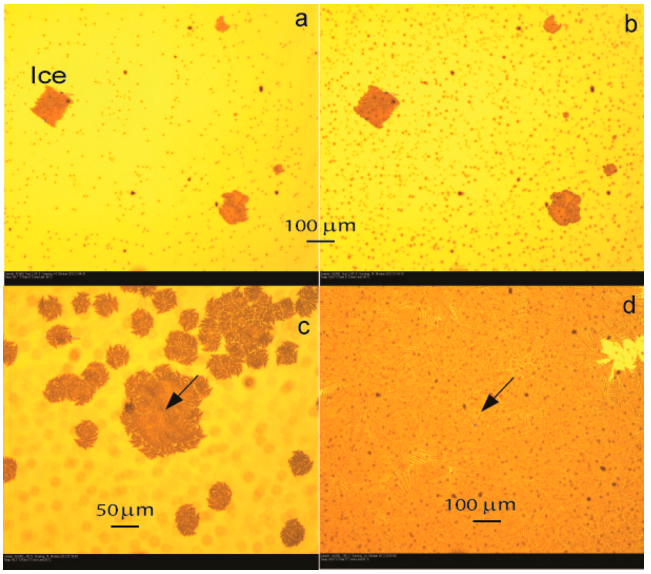

Figure 5. Optical cryo-microscope pictures of 62 wt % CA solution taken during cooling and subsequent warming. (a,b) Pictures are taken upon cooling at 216 and 193 K, respectively. Incipient ice crystallization is seen as brown dendritic crystals. Numerous dark spots are ice crystals nucleated on a cover glass by vapor deposition. (c,d) Pictures are taken upon warming at 220 and 230 K, respectively, where nucleation and ice growth occur most strongly. Arrows show ice crystals formed during the incipient freezing upon cooling.

demonstrate how ice develops upon cooling and subsequent warming of 62 wt % CA solution. According to the cooling thermogram in Figure 3, the tiny exotherm indicating incipient freezing starts at ~223 K and ceases below ~210 K. Below this temperature the baseline is practically straight. Similarly, the pictures in Figure 5a,b demonstrate that between 216 and 193 K the ice indeed grows very slowly. According to the warming 62 wt % CA thermograms in Figure 4, the resumed ice growth in the HVL peaks between 220 and 230 K. Strong growth is also observed between 220 and 230 K in our OC-M measurements (cf. Figure 5c,d). By analogy to the phenomenology we observed upon cooling at T_f, phase separation into two freeze-concentrated solutions of different concentrations (FCS_1 and FCS_2) may also occur during the freezing at T_{cr} upon warming of the HVL. However, while FCS_1 and FCS_2 transform to glass upon continued cooling, they become more fluid upon continued warming.

The onset of liquid–glass transition at $T_{g,c} \approx 185$ K is clearly visible in the thermogram of 60 wt % CA (Figure 3). The ΔC_p step at $T_{g2,c} \approx 208$ K is subtle but nevertheless visible on the

dx.doi.org/10.1021/jp510331h | J. Phys. Chem. A 2015, 119, 4515–4523

inclined exotherm of the slow freezing process. The FCS_1–glass transition, $T_{g1,c}$, cannot be identified as it is completely concealed by the freezing T_f peak. However, this does not mean that the $T_{g1,c}$ transition is absent. In fact, it has to exist because the FCS_1 forms during ice crystallization just like for the other concentrations for which $T_{g1,c} \approx 220$ K can be identified. Thus, upon cooling of 60 wt % CA, besides the freezing event of T_f, three different liquid–glass transitions with the onset at $T_{g,c} \approx 185$ K, $T_{g2,c} \approx 208$ K, and $T_{g1,c} \approx 220$ K are produced. The three liquid–glass transitions require the existence of three liquid regions of different concentrations. How the two liquid regions of FCS_1 and FCS_2 are formed we described and demonstrated in videos in our recent work.[27] In addition to FCS_1 and FCS_2, the third region is a fraction of 60 wt % CA solution, which does not have enough time to freeze completely at the applied cooling rate of 3 K/min because of the steep increase of the viscosity of 60 wt % CA. Similar to $T_{g2,c}$ transition, which terminates the slow freezing of FCS_2 at ~208 K, the $T_{g,c}$ transition terminates the freezing of remaining 60 wt % CA at ~185 K.

A natural question may arise, namely, whether the formed three (or two if concentration is less than 60 wt % CA) liquid regions of different concentrations may exist long enough in order to produce three liquid–glass transitions in a sample of only ~5 μL by volume subjected to the cooling rate of 3 K/min. It will be shown in the next subsection of 3.2, that the CA/H_2O solutions subjected to the cooling rates as small as 0.5 and 0.1 K/min also produce two FCS_1–glass and FCS_2–glass transitions. This suggests that the main factor that determines the lifetime of the two/three FCS regions of different concentrations is viscosity, which governs the rate of molecular diffusion. Because of the limited rate of H_2O diffusion between the two/three FCS regions, a concentration gradient is established between them. However, the volume of concentration–transition regions is much smaller than that of two/three FCS regions, and consequently, their liquid–glass and glass–liquid transitions are not visible in the thermograms in Figures 3 and 4.

The existence of three liquid–glass transitions upon cooling of 60 wt % CA requires the existence of three reversible glass–liquid transitions upon warming. We mentioned above that the warming thermogram of 60 wt % CA in Figure 1 contains only two glass–liquid transitions, $T_{g,w}$ and $T_{g2,w}$, and a prolonged ice crystallization peak of T_{cr}. It is reasonable to assume that the third glass–liquid transition, namely, the reverse glass–FCS_1 transition, $T_{g1,w}$, is concealed by the prolonged T_{cr} peak. Most likely, the prolonged T_{cr} peak consists of two exothermic peaks, which are produced by the resumed slow freezing of FCS_2 and the resumed freezing of the unfrozen fraction of 60 wt % CA. To verify this assumption, we performed several additional DSC measurements of 60 wt % CA. The thermograms displayed in Figure 6 demonstrate that different amounts of 60 wt % CA remain unfrozen upon cooling of samples of similar mass (5.05, 5.74, and 5.64 mg). In the DSC method, peak areas are proportional to the amount of material undergoing a phase transition. It is seen that the area of the T_{cr} peak and, consequently, the amount of unfrozen 60 wt % CA decreases from top to bottom in Figure 6. At the same time, the ΔC_p step of $T_{g,w}$ transition decreases, whereas the T_{tr2} transition becomes more pronounced in the thermograms from top to bottom. Thus, the thermograms in Figure 6 demonstrate that the prolonged T_{cr} peak indeed indicates resumed freezing of FCS_2 and freezing of unfrozen 60 wt % CA. The former

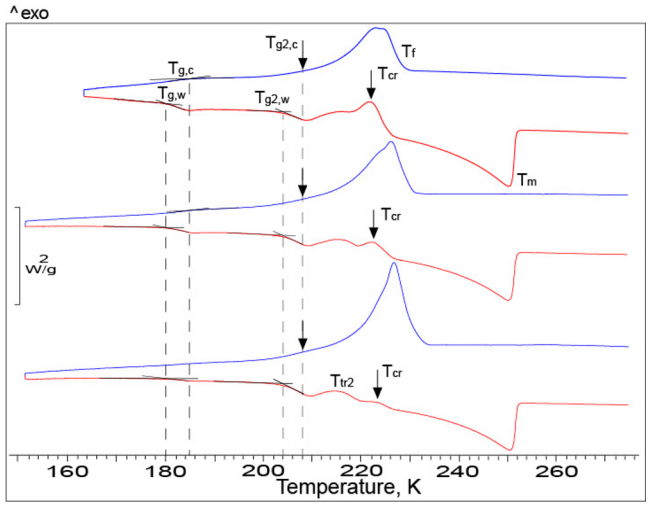

Figure 6. Cooling and warming thermograms of three 60 wt % CA drops. The upper thermograms are those from Figure 1. The middle cooling thermogram is that from Figure 3. The mass of drops, from which the upper, middle, and bottom thermograms were obtained, are 5.05, 5.74, and 5.64 mg, respectively. $T_{g,c}$ and $T_{g,w}$ mark the liquid–glass and reversible glass–liquid transitions of a fraction of 60 wt % CA, which does not freeze upon cooling. The remaining symbols have the same meaning as in Figure 4.

transition is at the origin of the exothermic feature of the T_{tr2} transition, whereas the latter is at the origin of the exothermic T_{cr} transition. Taking into account that the T_{tr2} transition is a net thermal effect produced by the resumed slow freezing of FCS_2 and reverse glass–FCS_1 transition, $T_{g1,w}$ (see discussion above and ref 27), we conclude that three reverse glass–liquid transitions with the onset at $T_{g,w} \approx 180$ K, $T_{g2,w} \approx 204$ K, and $T_{g1,w} \approx 217$ K are experienced upon warming of frozen 60 wt % CA. Note that there is a difference of about 3–4 K between the onset temperatures of liquid–glass transition observed upon cooling and reverse glass–liquid transition observed upon warming as illustrated in Figures 1, 3, 4, and 6. Thus, the total number of freezing events, which are observed upon cooling and warming of 60 wt % CA is three, namely, the freezing upon cooling, T_f, and the resumed freezing of FCS_2 and resumed freezing of the unfrozen 60 wt % CA upon warming.

3.2. Cooling and Warming of CA/H_2O at 0.1 and 0.5 K/min. To verify whether the applied cooling rate impacts the appearance and onset temperature of $T_{g1,w}$ and $T_{g2,w}$ transitions and, consequently, the concentration of FCS_1 and FCS_2 regions and mutual distribution of IF/(FCS_1 + FCS_2), we scanned 40 and 50 wt % CA solutions at cooling/warming rates as small as 0.5 and 0.1 K/min. Since the glass transition is a kinetic phenomenon, glass transition temperatures, T_g, shift upon changing rates, by contrast to transitions of thermodynamic origin such as melting. Here, it should be noticed that DSC measurements performed at small scanning rates are not only time-consuming but also produce a small signal-to-noise ratio that may disguise the ΔC_p step.[33] The rate dependence is summarized in Figures 7 and 8 for 50 and 40 wt % CA solutions, respectively. The thermograms obtained at 3 and 0.5 K/min are practically identical, i.e., the onset temperatures of T_f freezing event, liquid–glass $T_{g1,c}$, $T_{g2,c}$, and reverse glass–liquid $T_{g1,w}$, $T_{g2,w}$ transitions are practically the same (cf. Figure 7). Also the thermograms obtained at 0.5 and 0.1 K/min (cf. Figure 8) are practically identical. Although the ΔC_p step of $T_{g1,c}$ and $T_{g2,c}$ transitions disappears in the noise, the ΔC_p steps

dx.doi.org/10.1021/jp510331h | J. Phys. Chem. A 2015, 119, 4515–4523

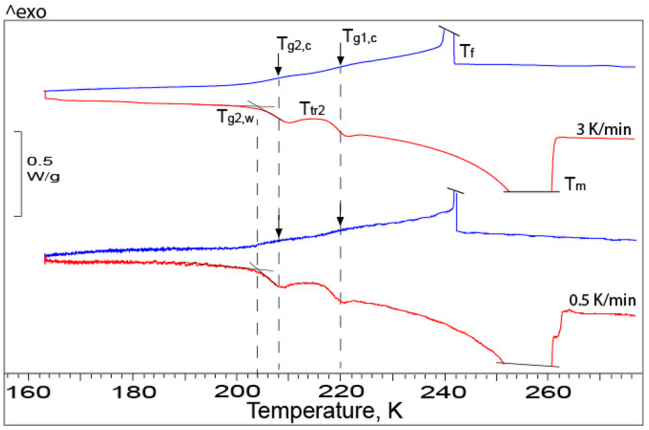

Figure 7. Comparison of cooling and warming thermograms obtained from two different drops of 50 wt % CA cooled/warmed at the scanning rate of 3 K/min (upper thermograms) and 0.5 K/min. The mass of drops are 6.22 mg (upper thermograms) and 6.35 mg. The upper thermograms are from Figure 1. All symbols have the same meaning as those in the Figures above.

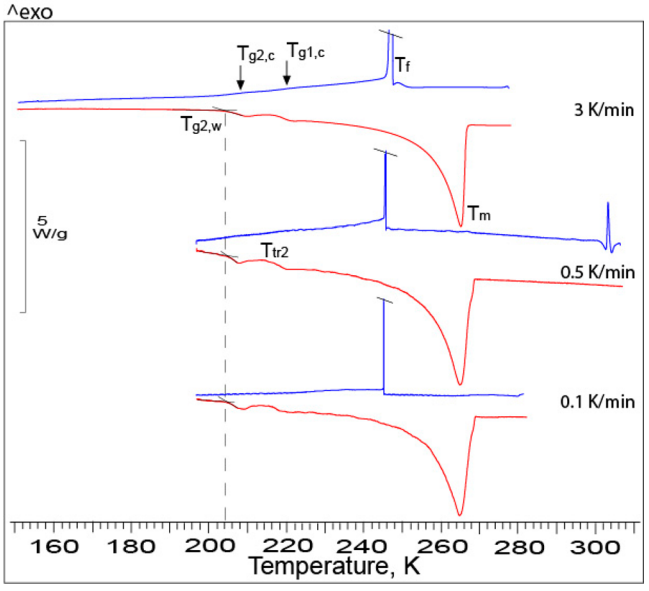

Figure 8. Comparison of 40 wt % CA thermograms obtained at the scanning rate of 3, 0.5, and 0.1 K/min. The upper thermograms are those from Figure 1. The middle thermograms are obtained at the cooling and warming rate of 0.5 K/min. The bottom cooling thermogram is obtained at 0.1 K/min and warming thermogram at 0.5 K/min. A sharp exothermic peak at ~305 K is due to the transition from anhydrous CA to CA-monohydrate.[35,36] All symbols have the same meaning as those in the Figures above.

of the reverse $T_{g1,w}$ and $T_{g2,w}$ transitions are clearly seen. The onsets of these glass transitions are practically unshifted. The constant onset temperatures of $T_{g1,c}$, $T_{g2,c}$ and $T_{g1,w}$, $T_{g2,w}$ transitions indicate that the applied cooling rate does not impact on the concentration of FCS_1 and FCS_2. Thus, the negligible differences between the thermograms obtained at different cooling rates suggest that the freezing process in *supercooled* CA/H_2O proceeds in the same way at 3 K/min and at 0.1 K/min. In other words, the concentration of FCS_1 and FCS_2 regions and mutual distribution of $IF/(FCS_1 + FCS_2)$ is *independent* of the applied cooling rate. Our OC-M observations of IF formed during freezing (not shown) suggest that the applied cooling rate also does not impact the morphology of IF, i.e., on the thickness and spatial distribution of dendritic ice branches/protuberances as long as the degree of solution supercooling before freezing is similar.

3.3. Quenching of CA/H_2O and Subsequent Warming at 3 K/min. We also investigated the impact of very large cooling rates on the freezing/thawing phenomenology. In particular, it is of interest to check whether vitrification or freezing takes place upon quenching. Furthermore, if freezing is still observed, it is of interest to check whether the appearance of $T_{g2,w}$ and T_{tr2} transitions and, consequently, the concentration of FCS_1 and FCS_2 regions and the mutual distribution of $IF/(FCS_1 + FCS_2)$ are affected. In Figure 9, we present

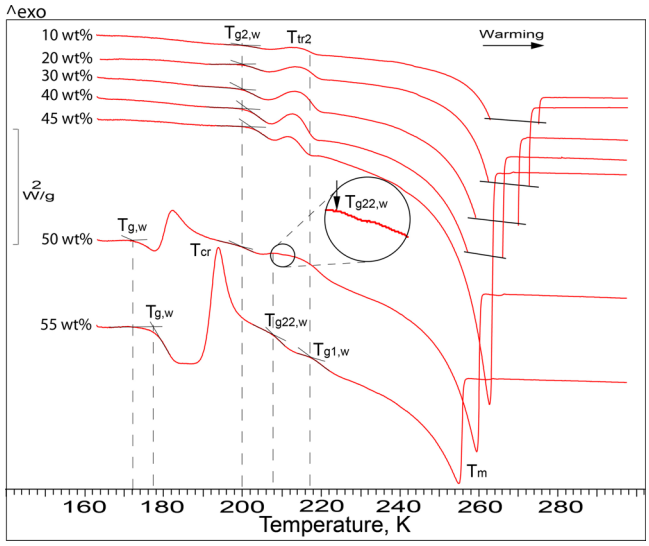

Figure 9. Warming thermograms of 10–55 wt % CA solutions quenched in liquid N_2. $T_{g,22w}$ and $T_{g,11w}$ mark glass–FCS_{22} and glass–FCS_{11} transitions (see text for details). The circle shows a magnification of the $T_{g,22w}$ transition in 50 wt % CA. Other symbols have the same meaning as those in previous Figures.

thermograms obtained upon warming of quenched 10–55 wt % CA. Similar to slowly cooled solutions (cf. Figure 4), also quenched 10–45 wt % CA solutions experience the $T_{g2,w}$ and T_{tr2} transitions. This implies that even at such high cooling rates (>100 K/s) freezing, not liquid–glass transition, occurs during quenching. Further, the comparison of Figures 4, 8, and 9 shows that the onset of $T_{g2,w}$ transition is down-shifted by ~1–4 K, and the shift is slightly larger for less concentrated solutions. This kind of shift is atypical of glassy aqueous solutions on increasing the cooling rate and scanning at the same, fixed heating rate.[52] In fact, faster cooling rates typically result in an upshift of the glass transition temperature rather than a down-shift because the supercooled liquid falls out of equilibrium at higher temperature when cooled at faster rates. A down-shift upon increasing the cooling rate violates this concept of fictive temperature[52] and indicates that the concentration of FCS_2 formed during quenching has to be slightly smaller than the concentration of FCS_2 formed at the cooling rate of 3, 0.5, and 0.1 K/min. The temperature region of the T_{tr2} transition becomes narrower and shifted ~2–3 K to colder temperature in comparison with that in Figures 4 and 8. As a result the onset of $T_{g1,w}$ transition is also shifted ~2–3 K to colder temperature, and the shift is slightly larger for more concentrated solutions. The shift of $T_{g1,w}$ suggests that in the

dx.doi.org/10.1021/jp510331h | J. Phys. Chem. A 2015, 119, 4515–4523

quenched solutions the concentration of FCS_1 is slightly smaller than that of FCS_1 formed at 3, 0.5, and 0.1 K/min cooling rates, i.e., the FCS_1 formed during quenching is *not* maximally freeze-concentrated.

Figure 9 shows that 50 and 55 wt % CA thermograms drastically differ from those of 10−45 wt % CA. In contrast to 10−45 wt % CA solutions, which freeze during quenching, the 50 and 55 wt % CA solutions partly and completely transform to glass, respectively. This vitrification upon quenching is inferred from the appearance of the $T_{g,w}$ transition, which is first followed by a short temperature window, in which the HVL exists, and finally followed by ice crystallization (T_{cr} peak). The ΔC_p step of the $T_{g,w}$ transition, the temperature window of HVL, and the area of the T_{cr} peak are smaller for the 50 wt % CA solution than for 55 wt % CA, in spite of similar drop masses, i.e., 5.61 and 5.78 mg, respectively. This implies that the former solution partly freezes and partly vitrifies. Further evidence that ice and, consequently, FCS_1 and FCS_2 are formed during the quenching of 50 wt % CA is the existence of the $T_{g2,w}$ and T_{tr2} transitions. The fact that the onset of the $T_{g2,w}$ transition is ∼4 K colder than that in Figure 4 indicates that the concentration of FCS_2 formed during quenching is less than that of FCS_2 formed at 0.1−3 K/min cooling rate. The smaller FCS_2 concentration results in lower viscosity and, consequently, colder onset temperature of the resumed freezing of FCS_2 (compare Figure 4). To verify whether there is a shift of the $T_{g1,w}$ transition, in Figure 10, we compare the 50 wt % CA

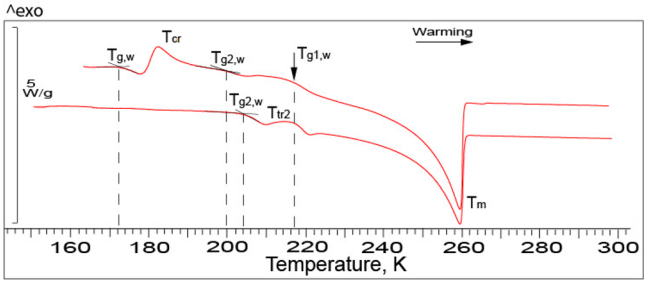

Figure 10. Comparison of the glass−liquid transition onsets in the warming thermograms of quenched (upper line, from Figure 9) and slowly cooled (3 K/min, bottom red line, from Figure 4) 50 wt % CA. All symbols have the same meaning as those in previous Figures.

thermograms from Figures 4 and 9. It is seen that there is no visible shift of the warmer part of the T_{tr2} transition, which, as we already know, contains the $T_{g1,w}$ transition. This fact suggests that there is no shift of the onset of the $T_{g1,w}$ transition and, consequently, the FCS_1 solution expelled from ice during the quenching of 50 wt % CA is *maximally* freeze-concentrated, i.e., of the same concentration as FCS_1 solution expelled from ice during freezing at slow cooling rates.

A unique feature in the freezing/thawing of CA solutions can be seen in the 55 wt % CA thermogram in Figure 9. It does not contain the exothermic feature of the T_{tr2} transition, but a massive T_{cr} peak. This indicates that no ice crystallizes upon quenching, and hence, no freeze-concentrated solutions form. Ice crystallizes, though, upon subsequent slow warming above $T_{g,w}$ when the formed HVL freezes (T_{cr} peak). This phenomenon of cold-crystallization itself is not unique, but known for many quenched substances, including the single-component system amorphous ice.[53] However, what is unique is the observation of two glass−liquid transitions above the cold-crystallization. The existence of *two* glass−liquid transitions upon warming at $T > T_{cr}$ requires the expulsion of two *glassy* solutions of different concentrations during cold-crystallization of ice at T_{cr}. That is, we put forward that freezing upon warming also produces two freeze-concentrated solutions. Judging from the onset of the $T_{g1,w}$ transition at ∼217 K, one of them is *maximally* freeze-concentrated, FCS_1 (cf. Figure 4), whereas the other (FCS_{22}) is less concentrated and transforms from glass to liquid at $T_{g22,w} < T_{g1,w}$. This phenomenology has the paradoxical implication that two distinct immobile, glassy solutions seem to be expelled upon cold-crystallization of ice. How can a glass be mobile enough to suddenly phase-segregate during freezing on the scale of micro- and millimeters? This mystery can easily be unraveled if we recall that the large amount of the latent heat of fusion associated with cold-crystallization at T_{cr} intermittently heats the freezing solution so that the freeze-concentrated solutions, FCS_{22} and FCS_1, are in the mobile, liquid state for a moment. As the freezing process decays between ∼194 and 198 K, the amount of emitted latent heat abruptly reduces and the sample temperature, and consequently, the temperature of FCS_{22} and FCS_1 start rapidly equilibrating with the environmental temperature due dissipation of heat to the environment. Since the environmental temperature at the T_{cr} cold-crystallization is much colder than the onset glass−liquid transition temperatures $T_{g22,c} \approx 211$ and $T_{g1,c} \approx 220$ K, the FCS_{22} and FCS_1 regions immediately transform to the glassy state after segregation. (We estimated the onset temperature of the FCS_{22}−glass transition as $T_{g22,c} \approx 211$ K because it should be ∼3−4 K warmer than the onset temperature of the reverse glass−FCS_{22} transition, which is $T_{g22,w} \approx 208$ K as is seen in Figure 9.) Signatures for the double FCS_{22}/FCS_1−glass transition at ∼194−198 K can not be seen in Figure 9 because they are masked by the latent heat evolution. However, its effects are clearly visible in the aftermath of the cold-crystallization event in the form of the anomalously elevated descending warm-side shoulder of the T_{cr} peak. In fact, the warm-side shoulder of the T_{cr} peak should have been lower than the baseline of HVL because the heat capacity of ice is less than that of water, and therefore, the height of the baseline lowers during freezing and increases during melting, as has been shown in Figure 7 in ref 26. The elevation of the warm-side shoulder of the T_{cr} peak is brought about by the large ΔC_p step of the double FCS_{22}/FCS_1−glass transition. That is, we suggest that also hidden liquid−glass transitions contribute to the complex phenomenology of CA solutions upon freezing and thawing. The formation of two FCSs (FCS_{22} and FCS_1) during the freezing upon warming to our best knowledge has never been reported before. (Note, the formation of *one* FCS during the freezing upon warming of quenched aqueous glycerol, ethylene glycol, sucrose, and glucose was observed for the first time by Luyet and Rasmussen[54] (see Figure 1 in ref 54); however, then this freeze-induced phase separation upon warming was not understood.) Thus, the total number of liquid−glass and glass−liquid transitions that occur during the warming of quenched-glassy 55 wt % CA solution is five, namely, $T_g \approx 177$ K, double FCS_{22}/FCS_1−glass transition in the temperature region of ∼194−198 K, $T_{g22,w} \approx 208$ K and $T_{g1,w} \approx 217$ K. Following this line of thought, the total number of liquid−glass and glass−liquid transitions is even six in the case of quenched 50 wt % CA solution, namely, $T_g \approx 172$ K, and double FCS_{22}/FCS_1−glass transition between ∼182 and 186 K (in the tail of the cold-crystallization peak), $T_{g2,w} \approx 200$ K, $T_{g22,w} \approx 208$ K, and $T_{g1,w} \approx 217$ K (cf. Figure 9). The

dx.doi.org/10.1021/jp510331h | J. Phys. Chem. A 2015, 119, 4515−4523

similarity of concentrations of freeze-concentrated solutions in quenched and slowly cooled CA solutions as well as the very similar morphology observed in OC-M experiments suggests that the degree of supercooling prior to the heterogeneous freezing event is very similar at all rates studied here.

4. CONCLUSIONS

In this work, we present the results of DSC and OC-M measurements of 10−64 wt % CA solutions subjected to different cooling/warming rates, including the quenching of DSC crucibles with a drop into liquid N_2. We observe in the cooling thermograms of 10−56 wt % CA one freezing event, T_f, and two FCS_1−glass and FCS_2−glass transitions at $T_{g1,c} \approx 220$ K and $T_{g2,c} \approx 208$ K, respectively. In the corresponding warming thermograms, we observe the reverse glass−FCS_2 transition at $T_{g2,w} \approx 204$ K, T_{tr2} transition, and prolonged ice melting event, T_m. The T_{tr2} transition is a net thermal effect produced by the reverse glass−FCS_1 transition at $T_{g1,w} \approx 217$ K and heat of fusion emitted during the resumed slow freezing of FCS_2.[27] In our OC-M measurements of 10−56 wt % CA, we are able to observe in situ how IF(FCS_1 + FCS_2) is formed during freezing and how ice (IF) melts during subsequent heating. We also observe the slow freezing of FCS_2 both upon cooling and subsequent warming of frozen solutions.[27]

In addition to the thermal events of 10−56 wt % CA, the cooling/warming thermograms of 60 wt % CA reveal a third liquid−glass transition, $T_{g,c}$, reverse glass−liquid transition, $T_{g,w}$, and cold-crystallization of ice, T_{cr}. These additional thermal events are due to the fraction of 60 wt % CA, which does not freeze but transforms to glass upon cooling. Upon cooling of 62 wt % CA, the cooling thermogram reveals only a subtle freezing, which indicates that practically all 62 wt % CA transforms to glass. Upon cooling of 64 wt % CA, there is no freezing but only a liquid−glass transition. Upon warming, glassy 62 and 64 wt % CA "melts" to the HVL at different $T_{g,w}$. Upon further warming, ice cold-crystallizes in the HVL at T_{cr} and then melts at T_m.

Upon warming of quenched 50 wt % CA, which partly freezes and partly transforms to glass during the quenching, we observe six liquid−glass and glass−liquid transitions and two freezing and one ice melting events. Upon warming of quenched 55 wt % CA, which completely transforms to glass during the quenching, we observe five liquid−glass and glass−liquid transitions and one freezing and one melting events. In these solutions, two FCS_{22} and FCS_1 are formed during the freezing upon warming, the finding that, to our best knowledge, was not reported before. We can only rationalize our observations when assuming a hidden double FCS_{22}/FCS_1−glass transition between ∼182 and 186 K and between ∼194−198 K for 50 and 55 wt % CA, respectively. Upon subsequent warming the glassy FCS_{22} and FCS_1 transform back to liquid at $T_{g22,w} \approx 208$ K and $T_{g1,w} \approx 217$ K, respectively.

The warming thermograms of slowly frozen 10−56 wt % CA and quenched 10−45 wt % CA are quite similar in the sense that both groups of thermograms contain $T_{g2,w}$ and T_{tr2} ($T_{g1,w}$) transitions. The only difference is that the $T_{g1,w}$ and $T_{g2,w}$ of quenched solutions (Figure 9) are slightly shifted to colder temperatures (Figures 4, 7, and 8). The minor change of $T_{g1,w}$ and $T_{g2,w}$ suggests that the concentration of FCS_1 and FCS_2 and IF/(FCS_1 and FCS_2) morphology are not sensitive to the applied cooling rate.

Our results, especially the finding that FCS_{22} and FCS_1 are formed during freezing upon warming, are the first of their kind, and provide a new look on the freezing and glass transition behavior of aqueous solutions. Our results can be used for the optimization of time- and energy-consuming lyophilization and freezing of foods and biopharmaceutical formulations and, consequently, for improving quality attributed to lyophilized products, among many other fields of science and applications where freezing plays a crucial role.

AUTHOR INFORMATION

Corresponding Author

*E-mail: anatoli.bogdan@uibk.ac.at.

Notes

The authors declare no competing financial interest.

ACKNOWLEDGMENTS

The authors are thankful for the financial support by the Austrian Science Fund FWF (project P23027). A.B. thanks Neumann, B., Morscher, W., Stadlober, M., Simonen, M., and Solasaari, J. for technical support, and the Physical and Chemical Departments of the University of Helsinki for providing facilities for the performance of DSC measurements.

REFERENCES

(1) Nordmann, C. E.; Weldon, A. S.; Patterson, A. L. X-Ray Crystal Analysis of the Substrates of Aconitase. II. Anhydrous Citric Acid. *Acta Crystallogr.* **1960**, *13*, 418−426.

(2) Mullin, J. W.; Leci, C. L. Evidence of Molecular Cluster Formation in Supersaturated Solutions of Citric Acid. *Philos. Mag.* **1969**, *19*, 1075−1077.

(3) Mullin, J. W.; Leci, C. L. Some Nucleation Characteristics of Aqueous Citric Acid Solutions. *J. Cryst. Growth* **1969**, *5*, 75−76.

(4) Timko, R. J.; Lordi, N. G. The Effect of Thermal History on the Transition Temperature of Citric Acid Glass. *J. Pharm. Sci.* **1979**, *71*, 1185−1186.

(5) Maltini, E.; Anese, M.; Shtylla, I. State Diagram of Some Organic Acid-Water Systems of Interest in Food. *Cryo Lett.* **1997**, *18*, 263−268.

(6) Daneshfar, A.; Baghlani, M.; Sarabi, R. S.; Sahraei, R.; Abassi, S.; Kaviyan, H.; Khezeli, T. Solubility of Citric, Malonic, and Malic Acids in Different Solvents From 302.2 to 333.2 K. *Fluid Phase Equilib.* **2012**, *313*, 11−15.

(7) Frank, H. V. Citric Acid. In *Ullmann's Encyclopedia of Industrial Chemistry*; Wiley-VCH: Weinheim, Germany, 2005.

(8) Caillet, A.; Puel, F.; Fevotte, G. In-line Monitoring of Partial and Overall Solid Concentration during Solvent-Mediated Phase Transition using Raman Spectroscopy. *Int. J. Phar.* **2006**, *307*, 201−208.

(9) Lu, Q.; Zografi, G. Phase Behavior of Binary and Ternary Amorphous Mixtures Containing Indomethacin, Citric Acid and PVP. *Pharm. Res.* **1998**, *15*, 1202−1206.

(10) Lu, Q.; Zografi, G. Properties of Citric Acid at the Glass Transition. *J. Pharm. Sci.* **1997**, *86*, 1374−1378.

(11) Izutsu, K.; Kadoya, S.; Yomota, C.; Kawanishi, T.; Yonemochi, E.; Terada, K. Freeze-Drying of Proteins in Glass Solids Formed by Basic Amino Acids and Dicarboxylic Acids. *Chem. Parm. Bull.* **2009**, *57*, 43−48.

(12) Kadoya, S.; Izutsu, K.; Yonemochi, E.; Terada, K.; Yomota, C.; Kawanishi, T. Glass-State Amorphous Salt Solids Formed by Freeze-Drying of Amines and Hydroxyl Carboxylic Acids: Effect of Hydrogen-Bonding and Electrostatic Interactions. *Chem. Pharm. Bull.* **2008**, *56*, 821−826.

(13) Sammers, M. P.; Enever, R. P. Preparation and Properties af Solid Dispersion System Containing Citric Acid and Primidone. *J. Pharm. Sci.* **1976**, *65*, 1613−1717.

(14) Timko, R. J.; Lordi, N. G. Thermal Characteristics of Citric Acid Solid Dispersions With Benzoic Acid and Phenobarbital. *J. Pharm. Sci.* **1979**, *681*, 601−605.

(15) Kueltzo, L. A.; Wang, W.; Randolph, T.; Carpenter, J. F. Effects of Solution Conditions, Processing Parameters, and Container Materials and Aggregation of a Monoclonal Antibody During Freeze-Drying. *J. Pharm. Sci.* **2008**, *97*, 1801−1812.
(16) Pikal-Cleland, K. A.; Rodriguez-Hornedo, N.; Amidon, G. L.; Carpenter, J. F. Protein Denaturation During Freezing and Thawing in Phosphate Buffer Systems: Monomeric and Tertrametric β-Galactosidase. *Arch. Biochem. Biophys.* **2000**, *384*, 398−406.
(17) Vijayarajkumar, P.; Choudhary, R. K.; Narne, R. Efavirenz Loaded Novel Citric Acid Dendritic Architecture for Increased Solubility and Sustained Delivery. *J. Pharm. Drug. Delivery Res.* **2012**, *1*, 1−5.
(18) Yang, J.; Webb, A. R.; Ameer, G. A. Novel Citric Acid-Based Biodegradable Elastomers for Tissue Engineering. *Adv. Mater.* **2004**, *16*, 511−516.
(19) Thomas, L. V.; Nair, P. D. (Citric Acid-co-Polycaprolactone Triol) Polyster A Biodegradable Elastomer for Soft Tissue Engineering. *Biomatter* **2011**, *1*, 81−90.
(20) Djordjevic, I.; Choudhury, N. R.; Dutta, N. K.; Kumar, S. Synthesis and Characterization of Novel Citric- Acid-Based Polyester Elastomers. *Polymer* **2009**, *50*, 1682−1691.
(21) Su, L.-C.; Xie, Z.; Zhang, Y.; Nguyen, K. T.; Yang, J. Study of the Antimicrobial Properties of Citrate-based Biodegradable Polymers. *Bioeng. Biotechnol.* **2014**, *2*, 1−9.
(22) Thomas, L. V.; Arun, U.; Remya, S.; Nair, P. D. A Biodegradable and Biocompatible PVA-Citric Acid Polysester with Potential Applications as Matrix for Vascular Tissue Engineering. *J. Mater. Sci: Mater. Med.* **2009**, *20*, S259−S269.
(23) Laguerie, C.; Aubry, M.; Couderc, J.-P. Some Physicochemical Data on Monohydrate Citrci Acid Solutions in Water: Solubility, Density, Viscosity, Diffusivity pH of Standard Solutions, and Refractive Index. *J. Chem. Eng. Data* **1976**, *21*, 85−87.
(24) Apelblat, A.; Manzurola, E. Solubility of Oxalic. Malonic, Succinic, Adipic, Maleic, Malic, Citric, and Tartaric Acids in Water from 278.15 to 338.15 K. *J. Chem. Thermodyn.* **1987**, *19*, 317−320.
(25) Bogdan, A.; Loerting, T. Impact of Substrate, Aging, and Size on the Two Freezing Events of $(NH_4)_2SO_4/H_2O$ Droplets. *J. Phys. Chem. C* **2011**, *115*, 10682−10693.
(26) Bogdan, A. Double Freezing of $(NH_4)_2SO_4/H_2O$ Droplets below the Eutectic Point and the Crystallization of $(NH_4)_2SO_4$ to the Ferroelectric Phase. *J. Phys. Chem. A* **2010**, *114*, 10135−10139.
(27) Bogdan, A.; Molina, M. J.; Tenhu, H.; Bertel, E.; Bogdan, N.; Loerting, T. Visualization of Freezing Process in Situ upon Cooling and Warming of Aqueous Solutions. *Sci. Rep.* **2014**, *4*, 7414.
(28) Ohgaki, K.; Hirokawa, N.; Ueda, M. Heterogeneity in Aqueous Solutions: Electron Microscopy of Citric Acid Solutions. *Chem. Eng. Sci.* **1992**, *47*, 1819−1823.
(29) Ohgaki, K.; Makihara, Y.; Morishita, M.; Ueda, M.; Hirokawa, N. Solute Clusters in Aqueous Citric Acid Solutions. *Chem. Eng. Sci.* **1991**, *46*, 3283−3287.
(30) Van Druden, M. A.; Finsy, R.; Merkus, H. G.; Scarlett, B.; van Rosmalen, G. M. Measurements of Cluster Formation in Aqueous Citric Acid Solutions by Proton Correlation Spectroscopy. *J. Cryst. Growth* **1993**, *134*, 196−202.
(31) Larson, M. A.; Garside, J. Solute Clustering in Supersaturated Solutions. *Chem. Eng. Sci.* **1986**, *41*, 1285−1289.
(32) Ginde, R. M.; Mayerson, A. S. Cluster Size Estimation in Binary Supersaturated Solutions. *J. Cryst. Growth* **1992**, *116*, 41−47.
(33) Höhne, G.; Hemminger, W.; Flammershain, H.-J. *Differential Scanning Calorimetry*; Springer: Berlin, Germany, 1995.
(34) Bogdan, A. Reversible Formation of Glassy Water in Slowly Cooling Diluted Drops. *J. Phys. Chem. B* **2006**, *110*, 12205−12206.
(35) Caillet, A.; Rivoire, A.; Calva, J.-M.; Puel, F.; Fevotte, G. Crystallization of Monohydrate Citric Acid. 1. In Situ Monitoring through the Joint Use of Raman Spectroscopy and Image Analysis. *Cryst. Growth Des.* **2007**, *7*, 2080−2087.
(36) Groen, H.; Roberts, K. J. Nucleation, Growth, and Pseudo-Polymorphic Behavior of Citric Acid as Monitored in Situ by Attenuated Total Reflection Fourier Transform Infrared Spectroscopy. *J. Phys. Chem. B* **2001**, *105*, 10723−10730.
(37) Liu, H.; Lelièvre, J. Transitions in Frozen Gelatinized-Starch Systems Studied by Differential Scanning Calorymetry. *Carbohydr. Polym.* **1992**, *19*, 179−183.
(38) Levine, H.; Slade, L. A Polymer Physic-Chemical Approach to the Study of Commercial Starch Hydrolysis Products (SHPs). *Carbohydr. Polym.* **1986**, *6*, 213−244.
(39) Levine, H.; Slade, L. Thermomechanical Properties of Small-Carbohydrate-Water Glasses and 'Rubbers'. *J. Chem. Soc., Faraday Trans.* **1988**, *84*, 2619−2633.
(40) Goff, H. D.; Verespej, E.; Jermann, D. Glass Transitions in Frozen Sucrose Solutions are Influenced by Solute Inclusions within Ice Crystals. *Thermochim. Acta* **2003**, *399*, 43−55.
(41) Ablett, S.; Izzard, M. J.; Lillford, P. J. Differential Scanning Calorimetric Study of Frozen Sucrose and Glycerol Solutions. *J. Chem. Soc., Faraday Trans.* **1992**, *88*, 789−794.
(42) Abblett, S.; Clark, A. H.; Izzard, J.; Lillford, P. J. Modeling of Heat Capacity-Temperature Data for Sucrose-Water Systems. *J. Chem. Soc., Faraday Trans.* **1992**, *88*, 795−802.
(43) MacKenzie, A. P. Non-Equilibrium Freezing Behavior of Aqueous Solutions. *Philos. Trans. R. Soc. London* **1977**, *278*, 167−189.
(44) Goff, H. D. The Use of Thermal Analysis in the Development of a Better Understanding of Frozen Food Stability. *Pure Appl. Chem.* **1995**, *67*, 1801−1808.
(45) Izzard, M. J.; Ablett, S.; Lillford, P. J.; Hill, V. L.; Groves, I. F. A Modulated Differential Scanning Calorimetric Study: Glass Transitions Occuring in Sucrose Solutions. *J. Therm. Anal.* **1996**, *47*, 1407−1418.
(46) Inoue, C.; Suzuki, T. Enthalpy Relaxation of Freeze Concentrated Sucrose-Water Glass. *Cryobiology* **2006**, *52*, 83−89.
(47) Schawe, J. E. K. A Quantitative DSC Analysis of the Metastable Phase Behavior of the Sucrose-Water System. *Thermochim. Acta* **2006**, *451*, 115−125.
(48) Goff, H. D.; Sahagian, M. E. Glass Transitions in Aqueous Carbohydrate Solutions and their Relevance to Frozen Food Stability. *Thermochim. Acta* **1996**, *280/281*, 449−464.
(49) Sacha, G. A.; Nail, S. L. Thermal Analysis of Frozen Solutions: Multiple Glass Transitions in Amorphous Systems. *J. Pharm. Sci.* **2009**, *98*, 3397−3405.
(50) Chang, L.; Milton, N.; Rigsbee, D.; Mishra, D. S.; Tang, X. (C).; Thomas, L. C.; Pikal, M. J. Using Modulated DSC to Investigate the Origin of Multiple Thermal Transitions in Frozen 10% Sucrose Solutions. *Thermochim. Acta* **2006**, *444*, 141−147.
(51) Shalaev, E. Y.; Franks, F. Structural Glass Transitions and Thermophysical Processes in Amorphous Carbohydrates and Their Supersaturated Solutions. *J. Chem. Soc. Faraday Trans.* **1995**, *91*, 1511−1517.
(52) Moynihan, C. T.; Easteal, A. J.; DeBolt, M. A.; Tucker, J. Dependence of the Fictive Temperature of Glass on Cooling Rate. *J. Am. Ceram. Soc.* **1976**, *59*, 12−16.
(53) Kohl, I.; Bachmann, L.; Hallbrucker, A.; Mayer, E.; Loerting, T. Liquid-Like Relaxation in Hyperquenched Water at ≤140 K. *Phys. Chem. Chem. Phys.* **2005**, *7*, 3210−3220.
(54) Luyet, B.; Rasmussen, D. Study by Differential Thermal Analysis of the Temperatures of Instability of Rapidly Cooled Solutions of Glycerol, Ethylene Glycol, Sucrose and Glycose. *Biodynamica* **1968**, *10*, 167−191.